Electronic structure of vacancy-type defects in hexagonal boron nitride

© *T.V. Perevalov* [1], *V.A. Gritsenko* [1,2], *A.V. Bukhtiyarov* [3], *I.P. Prosvirin* [3]

[1] Rzhanov Institute of Semiconductor Physics, Siberian Branch, Russian Academy of Sciences,
Novosibirsk, Russia
[2] Boreskov Institute of Catalysis, Siberian Branch of RAS,
Novosibirsk, Russia
[3] Novosibirsk State Technical University,
N Novosibirsk, Russia

E-mail: timson@isp.nsc.ru

The electronic structure of vacancy-type defects in hexagonal boron nitride (h-BN) synthesized by chemical vapor deposition, promising for microelectronics, is studied. The research is carried out using X-ray photoelectron spectroscopy and a simulation within the density functional theory. It is shown that the h-BN bombardment with argon ions leads not only to the near-surface layer cleaning from organic pollutants, but also to the generation of a high intrinsic defects concentration, mainly boron-nitrogen divacances. The greater the boron-nitrogen divacances concentration is, the longer the bombardment time is. The boron-nitrogen divacansion in h-BN is a significantly more energetically favorable defect than that of isolated boron and nitrogen vacancies. It is concluded that the most probable diamagnetic vacancy-type defects capable of participating in localization and, as a consequence, in charge transport in h-BN films is the boron-nitrogen divacancy.

Keywords: boron nitride (BN), photoelectron spectroscopy (XPS), quantum chemical simulation, density functional theory (DFT).

1. Introduction

Hexagonal boron nitride (h-BN) is a two-dimensional (2D) material with a layered crystal structure of graphite-like networks, one above the other with alternating boron and nitrogen atoms across the layers. h-BN is a promising material for use as a dielectric in various microelectronic devices due to such properties as a large band gap $(5.5-5.95 \, \text{eV})$ [1,2], high resistivity $(10^{12}-10^{14} \, \Omega \cdot \text{cm})$, heat resistance, non-toxicity, chemical inertness, stability of dielectric characteristics in the entire frequency range [3].

The electrophysical properties of h-BN are determined by the presence and properties of defects, which are inevitably present in real films. Defects in thin dielectric layers determine the reliability and often the performance of electronic devices. When h-BN is synthesized using industry-compatible methods such as Chemical Vapor Deposition (CVD), the concentration of defects (vacancies and lattice distortions) is higher than in mechanically exfoliated h-BN [4]. Defects in h-BN can lead to the formation of levels in the band gap and thus contribute to leakage currents and deterioration in the characteristics of devices based on it [5]. At the same time, defect-related electronic phenomena observed in CVD-grown h-BN, such as reversible resistive switching [6] and electrosynaptic plasticity [7] may be useful for designing resistive random access memories and electronic synapses for neuromorphic systems. Therefore, understanding the atomic and electronic structure of intrinsic defects in h-BN synthesized by the CVD method is an urgent task for the manufacture of microelectronic devices based on it.

One of the experimental methods for studying the electronic structure of defects in solids is X-ray photoelectron spectroscopy (XPS). However, this method is sensitive only to a high concentration of defects. A possible way to generate a high concentration of intrinsic defects, mainly vacancies, is to irradiate (bombard) the sample with argon ions. In most cases, bombardment with Ar^+ ions is used to clean the film surface from impurities and for layer-by-layer analysis. At the same time, for a number of oxide dielectrics (HfO_2 [8], ZrO_2 [9], Ta_2O_5 [10], TiO_2 [11]) this is also a method of oxygen depletion of films, i.e. the formation of oxygen vacancies and polyvacancies. The change in the chemical composition as a result of bombardment with Ar^+ ions can be judged with a high degree of accuracy by comparing the experimental and XPS of the valence band calculated ab initio [12,13]. For example, for Ta_2O_5 [13] this approach enabled to establish the expected and predicted oxygen depletion from transport measurements and to determine the atomic ratio [O]/[Ta] in the situation where the analysis XPS of core lines predicted the stoichiometric oxide. The most probable intrinsic defects in h-BN formed as a result of bombardment with Ar^+ ions are boron vacancies (V_B), nitrogen vacancies (V_N) and divacancies boron-nitrogen (V_{NB} — pair of closest to each other V_N and V_B). The electronic structure of intrinsic defects

in h-BN was previously studied using quantum chemical simulation [14–16], but only for the case of isolated defects (i.e. for their low concentration).

The aim of this study is to study the atomic and electronic structure of intrinsic defects in h-BN CVD films induced by argon ion bombardment using X-ray photoelectron spectroscopy and quantum chemical modeling.

2. Samples and measurement procedure

Multilayer h-BN about 7 nm thick was grown on „Graphene–Supermarket" polycrystalline copper foil 20 μm thick by the CVD method. The synthesis procedure is described in [17].

The XPS measurements were carried out on the spectrometer of the RGBL station of the BESSY II Synchrotron Research Center (Berlin, Germany). Spectral regions B1s, N1s, C1s and O1s were recorded at photoelectron kinetic energy 600 eV, and the valence band — at energies 300 and 600 eV. Spectra C1s ($E_b = 284.8$ eV were used to calibrate the binding energies. The atomic ratios of the elements were determined based on the integral intensities of the corresponding peaks, taking into account the photoionization cross sections. The intensities of the spectra were normalized to the corresponding coefficients determined based on the calibration spectra Au4f from gold foil. The analysis and deconvolution of the spectra into individual components were performed using the XPSPeak 4.1 program. The depth of analysis was estimated as 3 photoelectron mean free path lengths λ, which was calculated using the QUASES-IMFP-TPP2M program, and amounts to h-BN 33 and 54 Å for photoelectron kinetic energies of 300 and 600 eV, respectively. After recording the spectra of the original sample, its surface was bombarded with argon ions using an IQE-11/35 ion gun (accelerating voltage of 1.25 kV, current density of 3−4 μA/cm^2) with a total time of 5 and 50 min. It has been established that, at these parameters, there is no intense etching of the film.

Ab-initio simulation of the atomic and electronic structure of h-BN with inherent defects of the vacancy type (V_B, V_N and V_{NB}) was carried out in the Quantum ESPRESSO software package in the framework of the density functional theory [18]. The structural relaxation was calculated using the local exchange-correlation functionality (ECF) of the PBEsol parametrization, and the electronic structure was calculated using the non-local hybrid ECF HSE. The calculations were carried out in a 3D- model of periodic supercells, with a basis set of plane waves with a cutoff energy of 80 Ry, and the core was taken into account through optimized norm-preserving Vanderbilt pseudopotentials. To simulate the electronic structure of intrinsic defects in h-BN, we used supercells obtained by translation of a primitive 4-atom cell h-BN ($P63/mmc$). XPS of the h-BN valence band with different defect concentrations were modeled using supercells of 48 (translation $3 \times 2 \times 2$), 72 ($3 \times 3 \times 2$) and 200 ($5 \times 5 \times 2$) atoms. In the case of a 200-atomic

supercell, the defects can already be considered isolated from each other. The calculated XPS were obtained by summing the projection density of states (PDOS) spectra with weight factors equal to the corresponding values of the photoionization cross section and subsequent Gaussian smoothing of the spectrum with $\sigma = 1.0$ eV.

3. Results and discussion

The XPS -spectrum of the studied h-BN sample demonstrates the presence of intense peaks characteristic of boron, nitrogen, carbon and oxygen, while the signal from other elements is not observed within the sensitivity of the method (Fig. 1). The XPS-spectra of B1s and N1s for the initial film has a nonsymmetric Gaussian shape typical for h-BN with maxima at a binding energy of 190.4 eV for B1s and 398.3 eV for N1s [19–23], which refer to N−B bonds and are typical for boron and nitrogen in h-BN (Fig. 1, a, b). The presence of low-intensity B1s and N1s peaks on the side of high binding energies (191.6 and 399.6 eV, respectively) is due to the presence of oxygen and carbon in the analysis zone, which form bonds O−B, O−N and C−N [19–22].

As a result of the bombardment of the sample with Ar$^+$ ions, the measured XPS peaks broaden, the greater the broadening, the longer the bombardment time. This indicates disordering of the near-surface layer (creation of defects). As factors influencing the broadening of photoelectron peaks, the presence of the effect of recharging the sample due to the action of synchrotron radiation cannot be ruled out. The full peak widths at half height (FPWHH) for the XPS-spectrum B1s of the 190.4 eV line are 1.41, 1.67, and 1.96 eV, and of the 191.6 eV line — 1.57, 1.91 and 2.05 eV for the initial film bombed for 5 min and 50 min. respectively. Similarly, for the XPS-spectrum N1s, the FPWHH values for the 398.3 eV are 1.47, 1.69 and 1.84 eV, and for the 399.6 eV line — 1.66, 2.02 and 2.08 eV. Broadening of B1s and N1s mainly towards lower or higher binding energies is not observed. This indirectly indicates that, as a result of bombardment with Ar$^+$ ions, there is no predominant generation of boron or nitrogen vacancies, but the generation of boron-nitrogen divacancies is probable.

At the same time, as can be seen from the analysis of the atomic composition of the sample presented in Table 1, as a result of bombardment with Ar$^+$ ions, the nitrogen content slightly decreases: the atomic ratio [N]/[B] decreases

Table 1. Surface composition (at.%) and atomic ratios of elements for sample h-BN according to XPS ($KE = 600$ eV)

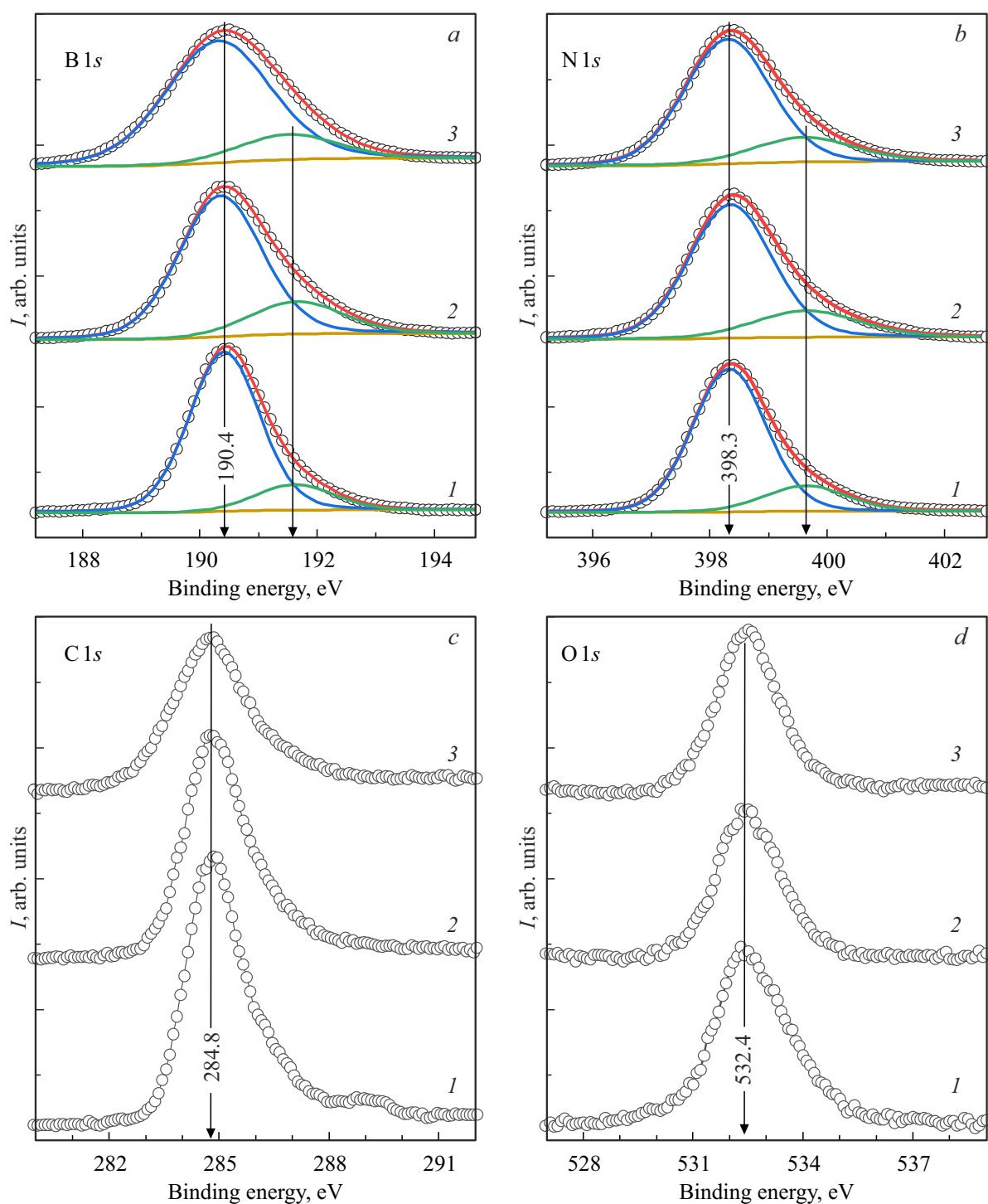| Sample	B, %	N, %	O, %	C, %	N/B
Initial	40.4	38.6	16.4	4.6	1.05
Ar$^+$ — 5 min	43.3	42.0	11.5	3.2	1.03
Ar$^+$ — 50 min	43.1	44.8	9.4	2.7	0.96

Figure 1. XPS spectra of B1s (*a*), N1s (*b*), C1s (*c*) and O1s (*d*) of the sample h-BN, measured at a photoelectron kinetic energy of 600 eV of the original sample (1) and after its bombardment with argon ions for 5 (2) and 50 (3) min.

with an increase in the duration of the bombardment. This may indicate the generation of nitrogen vacancies, however, this statement is doubtful, due to a slight decrease in the value of [N]/[B] even after 50 min bombardment and a typical error of the XPS method in quantitative analysis of about 5%, and besides, it contradicts the result of the almost symmetric broadening of the B1s and N1s spectra,

as well as the fact that the formation energy V_N is greater than V_B (Table 2). At the same time, XPS data do not contradict the assumption about the predominant generation of divacancies B−N.

Also, after the bombardment of the sample, a decrease in the intensity of the signal from carbon- and oxygen-containing functional groups is observed (lines 191.6
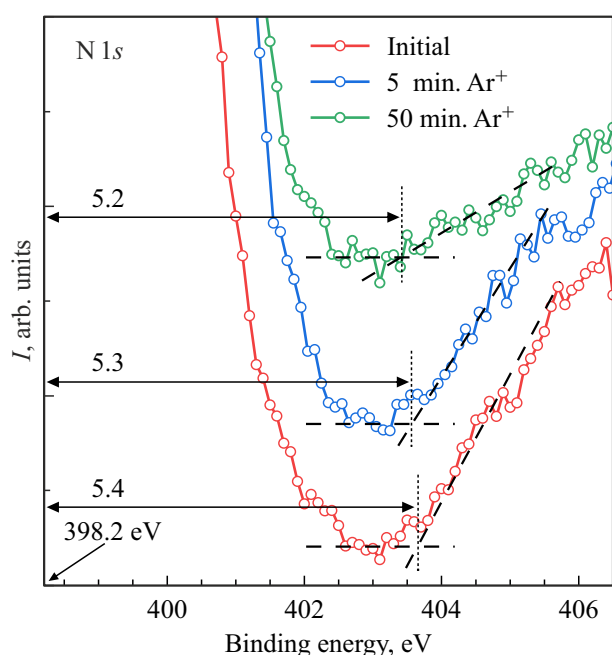
Figure 2. A fragment of the XPS-spectrum of N1s, illustrating the method for determining the values E_g of the initial h-BN film and after bombardment with Ar$^+$ ions for 5 and 50 min.

and 399.6 eV in Fig. 1). This is due to the partial removal of carbon and oxygen from the surface of the sample as a result of bombardment. The XPS-spectra of C1s demonstrate a noticeable decrease in the intensity of the peak with increasing bombardment duration, while the intensity of O1s decreases slightly, but the width of the peak O1s decreases. The fact of removal of carbon and oxygen is also reflected in the analysis of the elemental composition of the original and bombed samples (Table 1). Argon ion bombardment for 50 min. leads to a decrease in the concentration of oxygen from 16.4 to 9.4%, and carbon from 4.6 to 2.7%. A relatively high oxygen content is a characteristic feature of h-BN CVD films, which adsorb moisture from the air. Note that the storage and transportation of the test sample was carried out in a special evacuated bag.

Photoelectrons with N1s (as well as B1s) levels, passing through the h-BN layer, lose part of their kinetic energy to excite interband electron transitions, and the spectrum of these losses is reflected by the corresponding XPS -spectra.

Table 2. Formation energies (in eV) of neutral vacancies B and N, as well as divacancies B$-$N in a crystal h-BN, calculated for supercells 48, 72 and 00 atoms

Cell	$V_{\rm B}$	$V_{\rm N}$	$V_{\rm BN}$
48 at.	8.6 (8.1)	10.8 (10.1)	10.9 (10.6)
72 at.	8.4 (8.0)	10.8 (10.3)	12.9 (12.1)
200 at.	8.4 (7.9)	10.9 (10.3)	12.6 (11.9)

At the edge of this loss spectrum, by its linear interpolation to the background level, the value of the band gap E_g h-BN is estimated (Fig. 2). For the original sample, this method gives the value $E_g = 5.4$ eV, which is consistent with the value 5.5 eV [2], but less than 5.9 [1]. It is quite possible that the obtained value E_g for the studied sample is underestimated due to the relatively high oxygen content [24]. After bombardment with Ar$^+$ ions for 5 min, the value E_g is 5.3 eV, and for 50 min — 5.2 eV. Note that the change E_g as a result of bombarding the sample with Ar$^+$ ions is not greater than the accuracy of the method, the error of which is caused by the arbitrary selection of the background level and the range of the loss spectrum for linear interpolation.

An increase in the concentration of $V_{\rm B}$, $V_{\rm N}$ and $V_{\rm NB}$ in h-BN leads to an increase in the interaction of defects, which is reflected in the change in the position and width of the defect levels in the band gap, as can be seen from the total density of states (TDOS) spectra (Fig. 3). Regardless of the concentration, $V_{\rm B}$ and $V_{\rm N}$ are paramagnetic, while $V_{\rm BN}$ are diamagnetic defects. $V_{\rm B}$ and $V_{\rm N}$ form empty spin-polarized levels in the band gap h-BN, while $V_{\rm BN}$ gives the filled level near the top of the valence band. The presence of levels in the band gap indicates that vacancy-type defects in h-BN are capable of participating in charge localization and transport processes. For a supercell of 48 atoms, $V_{\rm BN}$ leads to a noticeable shift of the top of the valence band into the band gap. For a supercell of 200 atoms, defects form narrow peaks in the band gap, which indicates the localization of defect states in space and the isolation of defects from each other.

As the defect concentration increases (supercell size decreases), the $E_{\rm form}$ $V_{\rm B}$ formation energy increases, $V_{\rm N}$ decreases, and for $V_{\rm BN}$, first an increase is observed (transition to a 72-atomic supercell), and then a sharp decrease (transition to a 48-atomic supercell) (Table 2). This trend is observed for $E_{\rm form}$ values calculated in two approximations: using ECF HSE and PBEsol, although the second method gives values approximately 0.5 eV less. The significant fact is that $E_{\rm form}$ $V_{\rm BN}$ is significantly less than the sum of $E_{\rm form}$ for $V_{\rm B}$ and $V_{\rm N}$, and for the 48-atom supercell $E_{\rm form}$ $V_{\rm BN}$ practically coincides with $E_{\rm form}$ $V_{\rm N}$. Using direct enumeration of possible mutual positions for the pair $V_{\rm B}$ and $V_{\rm N}$ in the h-BN crystal, it was found that the most energetically favorable configuration of their mutual arrangement is the immediate proximity, i.e. the divacancy B$-$N. This result is consistent with the data of [16], according to which $V_{\rm B}$ can migrate until it forms a more stable B$-$N divacancy. Thus, according to the results of *ab initio* simulations, the dominant defect of the vacancy type in h-BN is $V_{\rm BN}$.

The experimental and calculated *ab initio* XPS spectra of the h-BN valence band are shown in Fig. 4. First of all, it should be noted the good agreement between the calculated and experimental data on the width and position of the subbands, as well as on the relative intensity and number of peaks. Moreover, this agreement exists

despite the presence of signals from carbon and oxygen in the experimental spectra. Bombardment of the h-BN film with Ar^+ ions leads to broadening of the upper edge XPS of the valence band, and longer the bombardment time, the greater broadening. This means that, as a result of bombardment, defects are formed, which give filled levels near the edge of the valence band. Since the formation of B−N divacancies is more probable, it is for this type of defects in its various concentrations in h-BN XPS of the valence band are calculated (Fig. 4). In agreement with experiment, the calculated spectra also demonstrate the broadening of the valence band edge into the band gap with increasing defect concentration, in this case only V_{BN}.v From the qualitative correspondence of this broadening to the experimental data, we can conclude that in the film under study the concentration V_{BN} after bombardment for 5 min is 2−3 at.%, and for 50 min —
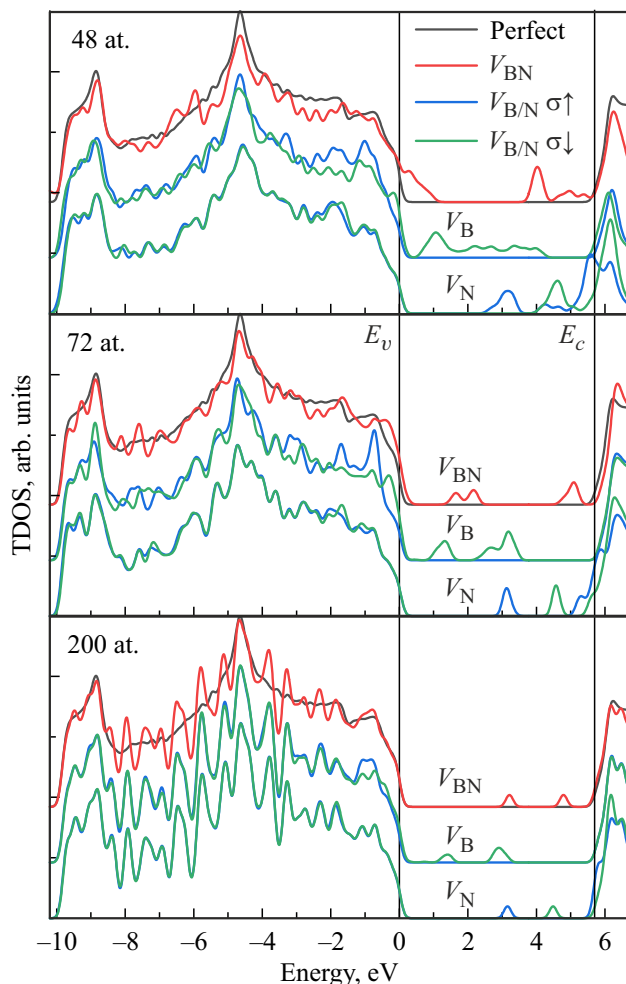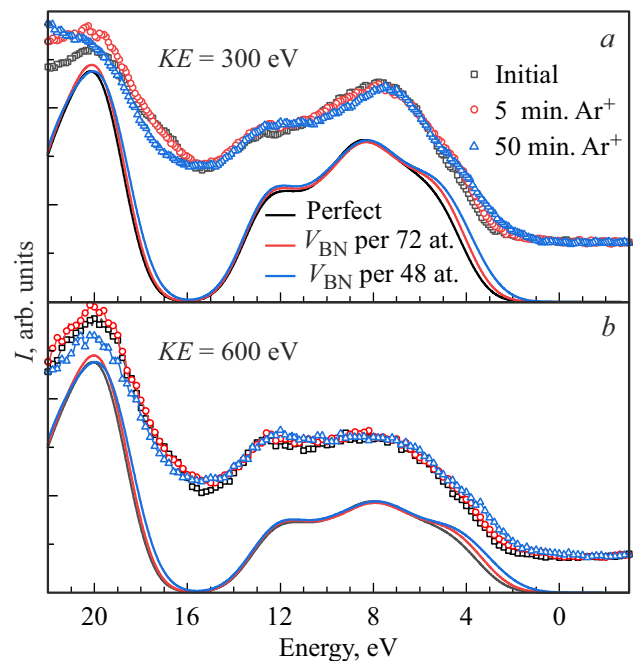

Figure 4. XPS -spectra of the valence band measured at photoelectron kinetic energies of 300 eV (*a*) and 600 eV (*b*) for the initial film h-BN and after bombardment with Ar^+ ions for 5 and 50 min (symbols), as well as the calculated spectra for h-BN with different concentrations V_{BN} (lines).

4−5 at.%. In addition, the above-described monotonic decrease in the band gap with increasing bombardment time can be explained by a shift of the valence band edge into the band gap.

4. Conclusion

In this article, it is shown that the bombardment of the h-BN CVD film with argon ions not only cleans the near-surface layer from organic contaminants, but is also a method of generating a high (on the order of 1 at.%) concentration of its own vacancy-type defects, predominantly boron-nitrogen divacancies (pairs of boron and nitrogen vacancies closest to each other). It is shown that the formation of boron-nitrogen divacancies in h-BN is much less energy-intensive than pairs of isolated boron and nitrogen vacancies, while the formation energy of a boron-nitrogen divacancy is close to that for an isolated nitrogen vacancy. An energetically favorable configuration of the mutual arrangement of boron and nitrogen vacancies is their close proximity (i.e. divacancy). It is shown that an increase in the concentration of divacancies B−N leads to a slight decrease in the band gap h-BN due to the broadening of the upper edge of the valence band. Calculations of the electronic structure have shown that boron-nitrogen divacancies are diamagnetic defects in h-BN, which form levels in the dielectric band gap, and thus are capable of participating in charge localization, leakage

Figure 3. TDOS h-BN spectra for a defect-free structure (black curves), structures with a boron V_B, and nitrogen V_N vacancies (blue curves — spin „up", green – spin „down"), and with boron-nitrogen V_{BN} divacancy (red curves) calculated using supercells of different sizes: (*a*) 48, (*b*) 72, and (*c*) 200 atoms. Zero energy corresponds to the position of the top of the valence band E_V.

currents, or formation of a conductive filament. It is shown that a comparison of the calculated and experimental X-ray photoelectron spectra not only reveals the boron-nitrogen divacancies as the dominant defect in h-BN films bombarded with argon ions, but also enables to estimate their concentration. The obtained results lead to the conclusion that the most probable defect of the vacancy type, which determines the electrical properties of h-BN CVD films, is the boron-nitrogen divacancy.

Acknowledgments

Funding

Conflict of interest

The authors declare that they have no conflict of interest.

References

[1] G. Cassabois, P. Valvin, B. Gil. Nature Photon. **10**, 262 (2016).

[2] L. Song, L.J. Ci, H. Lu, P.B. Sorokin, C.H. Jin, J. Ni, A.G. Kvashnin, D.G. Kvashnin, J. Lou, B.I. Yakobson, P.M. Ajayan. Nano Lett. **10**, 3209 (2010).

[3] M.Y. Li, S.K. Su, H.S.P. Wong, L.J. Li. Nature **567**, 169 (2019).

[4] K.S. Novoselov, V.I. Fal'ko, L. Colombo, P.R. Gellert, M.G. Schwab, K. Kim. Nature **490**, 192 (2012).

[5] H. Pandey, M. Shaygan, S. Sawallich, S. Kataria, W. Zhenxing, A. Noculak, M. Otto, M. Nagel, R. Negra, D. Neumaier, M.C. Lemme. IEEE Trans. Electron Dev. **65**, 4129 (2018).

[6] F. Hui, M.A. Villena, W.J. Fang, A.Y. Lu, J. Kong, Y.Y. Shi, X. Jing, K.C. Zhu, M. Lanza. 2D Mater. **5**, 031011 (2018).

[7] Y.Y. Shi, X.H. Liang, B. Yuan, V. Chen, H.T. Li, F. Hui, Z.C.W. Yu, F. Yuan, E. Pop, H.S.P. Wong, M. Lanza. Nature Electron. **1**, 458 (2018).

[8] A.A. Sokolov, A.A. Ovchinnikov, K.M. Lysenkov, D.E. Marchenko, E.O. Filatova. ZhTF **80**, 131 (2010) (in Russian).

[9] C. Morant, A. Fernandez, A.R. Gonzalezelipe, L. Soriano, A. Stampfl, A.M. Bradshaw, J.M. Sanz. Phys. Rev. B **52**, 11711 (1995).

[10] P.H. Holloway, G.C. Nelson. J. Vac. Sci. Technol. **16**, 793 (1979).

[11] T.V. Perevalov, D.R. Islamov, A.A. Saraev. Pisma v ZhTF, **42**, 97 (2016) (in Russian).

[12] T.V. Perevalov, R.M.Kh. Iskhakzai, V.Sh. Aliev, V.A. Gritsenko, I.P. Prosvirin. ZhETF **158**, 1083 (2020) (in Russian).

[13] V.A. Gritsenko, T.V. Perevalov, V.A. Voronkovskii, A.A. Gismatulin, V.N. Kruchinin, V.S. Aliev, V.A. Pustovarov, I.P. Prosvirin, Y. Roizin. ACS Appl. Mater. Int. **10**, 3769 (2018).

[14] A. Sajid, J.R. Reimers, M.J. Ford. Phys. Rev. B **97**, 064101 (2018).

[15] L. Weston, D. Wickramaratne, M. Mackoit, A. Alkauskas, C.G. Van de Walle. Phys. Rev. B **97**, 214104 (2018).

[16] A. Zobelli, C.P. Ewels, A. Gloter, G. Seifert. Phys. Rev. B **75**, 094104 (2007).

[17] K.K. Kim, A. Hsu, X.T. Jia, S.M. Kim, Y.M. Shi, M. Dresselhaus, T. Palacios. J. Kong, ACS Nano **6**, 8583 (2012).

[18] P. Giannozzi, O. Andreussi, T. Brumme, O. Bunau, M.B. Nardelli, M. Calandra, R. Car, C. Cavazzoni, D. Ceresoli, M. Cococcioni, N. Colonna, I. Carnimeo, A. Dal Corso, S. de Gironcoli, P. Delugas, R.A. DiStasio, A. Ferretti, A. Floris, G. Fratesi, G. Fugallo, R. Gebauer, U. Gerstmann, F. Giustino, T. Gorni, J. Jia, M. Kawamura, H.Y. Ko, A. Kokalj, E. Kucukbenli, M. Lazzeri, M. Marsili, N. Marzari, F. Mauri, N.L. Nguyen, H.V. Nguyen, A. Otero-de-la-Roza, L. Paulatto, S. Ponce, D. Rocca, R. Sabatini, B. Santra, M. Schlipf, A.P. Seitsonen, A. Smogunov, I. Timrov, T. Thonhauser, P. Umari, N. Vast, X. Wu, S. Baroni. J. Phys. Condens. Mater. **29**, 465901 (2017).

[19] S. Behura, P. Nguyen, S.W. Che, R. Debbarma, V. Berry. J. Am. Chem. Soc. **137**, 13060 (2015).

[20] H. Sediri, D. Pierucci, M. Hajlaoui, H. Henck, G. Patriarche, Y.J. Dappe, S. Yuan, B. Toury, R. Belkhou, M.G. Silly, F. Sirotti, M. Boutchich, A. Ouerghi. Sci Rep. **5**, 16465 (2015).

[21] S.S. Gao, Q.D. An, Z.Y. Xiao, S.R. Zhai, D.J. Yang. ACS Appl. Nano Mater. **1**, 5895 (2018).

[22] Z.H. Cui, A.J. Oyer, A.J. Glover, H.C. Schniepp, D.H. Adamson. Small **10**, 2352 (2014).

[23] A.T. Barton, R. Yue, S. Anwar, H. Zhu, X. Peng, S. McDonnell, N. Lu, R. Addou, L. Colombo, M.J. Kim, R.M. Wallace, C.L. Hinkle. Microelectron. Eng. **147**, 306 (2015).

[24] R.S. Singh, R.Y. Tay, W.L. Chow, S.H. Tsang, G. Mallick, E.H.T. Teo. Appl. Phys. Lett. **104**, 163101 (2014).